Time Evolution of Cosmic-Ray Modified Plane Shocks

H. Kang[1] and T.W. Jones[2]

[1] *Department of Earth Sciences, Pusan National University, Pusan 609-735, Korea*
[2] *Department of Astronomy, University of Minnesota, Minneapolis, MN 55455, USA*

Abstract

We have developed a novel computer code designed to follow the evolution of cosmic-ray modified shocks, including the full momentum dependence of the particles for a realistic diffusion coefficient model. In this form the problem is technically very difficult, because one needs to cover a wide range of diffusive scales, beginning with those slightly larger than the physical shock thickness. With most finite difference schemes for Euler's equations the numerical shock thickness is at least one zone across, so this provides a lower bound on the physical scale for diffusive transport computation. Our code uses sub-zone shock tracking (LeVeque & Shyue 1995) and multi-level adaptive mesh refinement to provide enhanced spatial resolution around shocks at modest cost compared to the coarse grid and vastly improved cost effectiveness compared to a uniform, highly refined grid. We present and discuss the implications from our initial results.

1   Introduction:

Diffusive shock acceleration is now widely accepted as the model to explain the production of cosmic rays (CR) in a wide range of astrophysical environments. Owing to complex nonlinear physics involved in the model, numerical simulations have been quite useful and successful in understanding the details of the acceleration process and dynamical feedback of the CRs to the underlying plasma. Accurate solutions to the CR diffusion-convection equation require a computational grid spacing much smaller than the diffusion lengths of the CR particles. In a realistic diffusion transport model, it is thought that the diffusion coefficient should have a steep momentum dependence, $\kappa(p) \propto p^s$, with $s \sim 1 - 2$. For the lowest energy particles the diffusion lengths are only slightly greater than the shock thickness, while they can be many orders of magnitude greater than that for the highest energy particles. Thus, a wide range of length scales is required to be resolved in order to solve the diffusion convection equation correctly for the model with a realistic diffusion coefficient. Especially the diffusion of particles whose mean free paths are a few times that of thermal particles determines the injection rate of the CRs in the so-called "thermal leakage" type injection model. Thus resolving these smallest scales is of critical importance in estimating the injection and acceleration efficiency. Previous numerical simulations which adopted the traditional flux-differencing method on a uniform grid were often forced to assume a weak momentum dependence (*e.g.* $s = 0.25$ in Kang & Jones 1991). Here we present a new hydro/CR code that can track exactly a shock wave as a discontinuous jump and use multiple levels of grid refinement around the shock.

2   Numerical Method:

2.1   Shock Tracking: The hydrodynamic conservation equations are solved in the 1D plane-parallel geometry by the wave-propagation algorithm described in LeVeque (1997). In this method a Riemann problem is solved at each interface between grid cells and the wave solutions (*i.e.* , speeds of waves and jumps associated with three wave modes) are used directly to update the dynamic variables at each cell. Within this method a shock-tracking algorithm of LeVeque & Shyue (1995) can be incorporated easily, since the Riemann solutions tell us exactly how the waves propagate. An additional cell boundary is introduced at the location of the shock, subdividing an uniform cell into two sub-cells. This cell boundary (shock front) is moved to a new location using the Riemann solutions (*i.e.* , $x_s^{n+1} = x_s^n + v_s \, \Delta t$) in the next time step and the waves are propagated onto the new set of grid zones. Since the new grid is chosen so that the shock wave is propagated exactly to cell boundaries, the shock remains as an exact discontinuity without smearing. One advantage of using

the wave-propagation method for the shock tracking scheme is that the large time step satisfying the Courant condition for the uniform grid can be used even if the shock is very close to the boundary of the uniform cell and so the sub-cell is much smaller than the uniform cell. The CR diffusion-convection equation is solved in two steps: 1) the diffusion term is solved by the Crank-Nicholson scheme as described in Kang & Jones (1991). 2) the advection term is solved by the wave-propagation method as for the gasdynamic variables.

2.2 Adaptive Mesh Refinement:
We also adopted the Adaptive Mesh Refinement (AMR) technique developed by Berger & LeVeque (1998).

Ideal gasdynamic equations in 1D planar geometry do not contain any intrinsic length scales to be resolved, but once the precursor due to the CR pressure modification becomes significant, the grid spacing should be fine enough to resolve the precursor structure. The CR diffusion-convection equation, however, involves a wide range of length scales corresponding to the diffusion lengths which can depend strongly on the particle momentum in realistic diffusion models. Compared to the general version of the AMR code of Berger & LeVeque (1998)
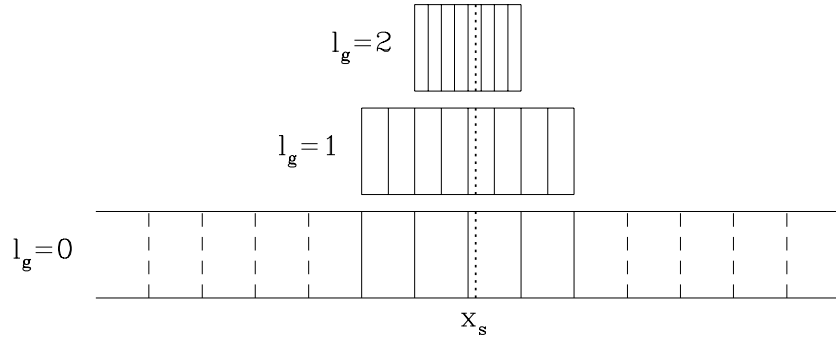

Figure 1: Layout of original grid and two refined grids. $N_{rf} = 4$ cells around the shock are refined by a factor of two. The shock is indicated by the dotted lines.

a much simpler scheme is sufficient for our needs, since we only need to refine the region around the shock whose location is exactly known in our shock-tracking code.

A fixed number of cells around the shock (N_{rf}) are identified as the "refinement region" on the 0-th level grid (*i.e.* , original uniform coarse grid). Then each cell is refined by a factor of two by placing $2N_{rf}$ cells within the refinement region at the 1st level grid. Then N_{rf} cells around the shock on the 1st level grid are chosen to be refined further to the 2nd level grid, making the length of the refinement region a half of that in the 1st level grid. The same refinement procedure is applied to higher level grids. So at all levels, there are $2N_{rf}$ cells around the shock, but the length of the computation domain is shrunk by a factor of 2 from the previous level. Fig. 1 shows an example of refined grid levels up to $l_g = 2$ with $N_{rf} = 4$. The refinement is done so that the shock remains near the middle of the computational domain at all levels. This is possible only because we know the exact location of the shock. The velocity in the refined grid is transformed so that the shock is at rest in the frame of the numerical simulation. This is to ensure that the shock remains near the middle of the computational domain at all grid levels during the time integration of one time step of the coarse grid. Thus the refinement region at all levels is moving along with the shock. Integration of the gasdynamic variables and advection of the CR distribution function are done by the wave-propagation method at each level grid. The detailed description of how to coordinate the time integration between levels and how to preserve global conservation at the interfaces between coarse and fine grids will be presented elsewhere. The basic idea applied for one level of refinement can be found in Berger & LeVeque (1998).

3 Simulation Results:

The dynamics of the CR modified shock depends on four parameters: the adiabatic index, $\gamma = 5/3$, gas Mach number of the shock, $M = V_s/c_s$, $\beta = V_s/c$, and the diffusion coefficient, where c_s and c are the upstream sound speed and the speed of light, respectively. For our simulations we consider $M = 20$, $\beta = 10^{-2}$, and two diffusion models, $\kappa_A = p^{0.525}$ and $\kappa_B = p$. The initial conditions in the rest frame of the shock for the

test problem are: $\rho_1 = 1.$, $P_{g,1} = 1.5 \times 10^{-3}$, $u_1 = -1.$ upstream and $\rho_2 = 4.$, $P_{g,2} = 7.5 \times 10^{-1}$, $u_2 = -0.25$ downstream. Here the velocities are normalized to the initial shock speed. We adopted the "thermal leakage" type injection model introduced in Kang & Jones (1995), in which the injection pool of particles are established by letting the particles with $p > c_1 p_{th}$ diffuse across the shock, where p_{th} is the thermal peak momentum and $c_1 = 2.8$ is a free parameter that limits the injection rate. The numerical domain is [-25,+75] and the number of cells, n, ranges from 1000 to 4000. The number of refined cells around the shock is $N_{rf} = 100$ on the original grid and so there are $2N_{rf} = 200$ cells on each refined level. For the κ_A model the diffusion length of p_{th} is $l_d = 0.09$, while it is $l_d = 0.01$ for the κ_B model. We used 230 logarithmic momentum zones in log(p/mc)=[-3.0,+3.0].

Fig. 2 shows how the particle distribution $(g(p) = f(p)\,p^4)$ at the shock evolves in time in our simulations with different grid spacings. There are 6 curves corresponding to $t = 10, 20, 30, 40, 50,$ and 60 in each panel. They show the typical Maxwellian distribution that peaks at $p_{th} = 10^{-2}$ and the CR particle distribution that asymptotes to a power-law as time increases. For $n = 1000$, the cell size $\Delta x = 0.1$ is too large for the diffusion of the particles in the injection pool to be treated correctly, so the injection and the acceleration are under-estimated. We note the results of $n = 2000$ and $l_g = 1$ are consistent with those of $n = 4000$ and $l_g = 0$, as expected. For the highest resolution case ($n = 2000$, $l_g = 3$), the CR pressure increases up to 13% of the postshock gas pressure and a weak precursor develops by the end of the simulation. The distribution reaches a power-law of p^4, but it flattens slightly at higher momentum since those particles can sample the total velocity jump, which is slightly greater than a factor of 4. The injection and the acceleration processes depend on the momentum dependence of the diffusion coefficient models. In the low energy regime, the particles in the injection pool have much smaller diffusion lengths in the κ_B model than in the κ_A model, so the injection is more severely underestimated in the κ_B model than in the κ_A model in a given spatial resolution. In the high energy regime, on the other hand, the cut-off at the high momenta sets in much more abruptly in the κ_B model than in the κ_A model due to the stronger momentum dependence of the acceleration time scale.

Figure 2: Time evolution of the distribution function $g = fp^4$ at $t = 10, 20, 30, 40, 50,$ and 60 from the simulations with different grid spacings and levels of refinement. κ_A model is used.

Fig. 3 shows how the CR pressure increases with time at different spatial resolutions for the same simulations shown in Fig. 2. The numerical frame is chosen so that the shock moves to the right with $u_s = 0.05$, if there is no modification due to CR pressure. It also demonstrates that injection and acceleration are much slower in
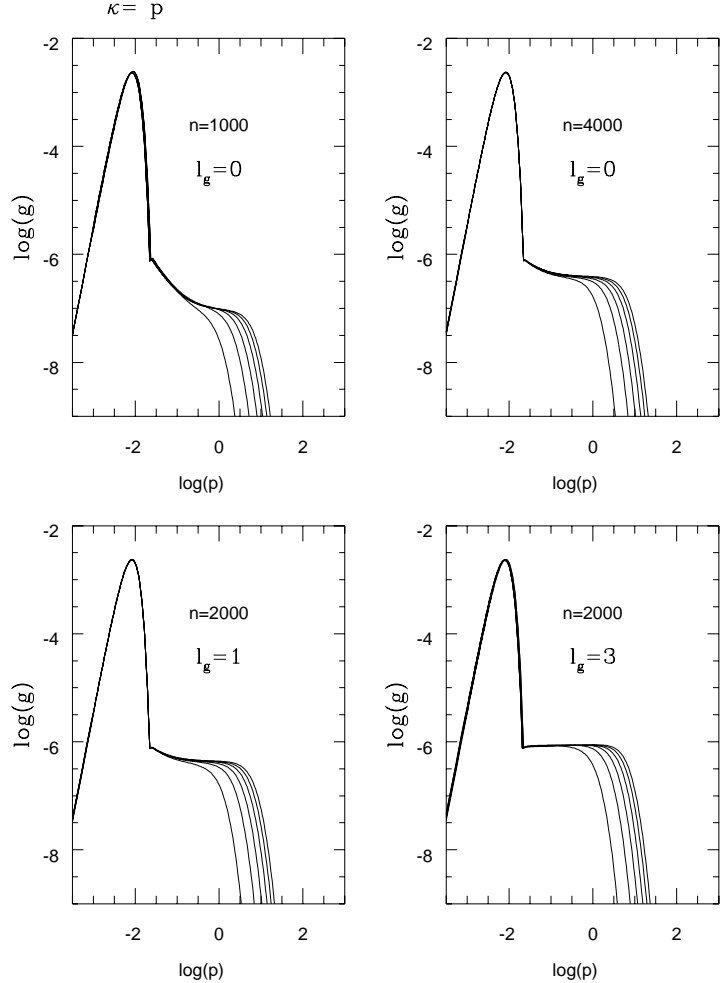
under-resolved simulations.

4 Summary:

We have developed a new hydro/CR dynamics code by incorporating the shock-tracking method and the Adaptive-Mesh-Refinement technique into a hydrodynamics code based on the wave-propagation method. By tracking the shock location exactly, we can refine the regions around the shock to an arbitrary level of refinements. The code has been applied to simulations of CR modified shocks with more realistic diffusion coefficient models which were not possible previously due to severe computational requirements. Some preliminary results from the time-dependent simulations have been presented here. The AMR technique we adopted proves to be very cost effective. In typical simulations considered here, for example, the computing time increases by factors of 1.5, 2.3, 4., 7. for the maximum refinement levels $l_g = 1, 2, 3, 4$, respectively, compared with the case of no refinement ($l_g = 0$). It should be compared with the time increases by factors of $(2^{l_g})^2$ for the simulations of an uniform grid spacing that matches the cell size at the $l_g - th$ refined level grid.

We thank Drs. R. LeVeque and K. Shyue for giving us their 1D shock-tracking code and helping us understand the basic concepts behind their AMR technique.
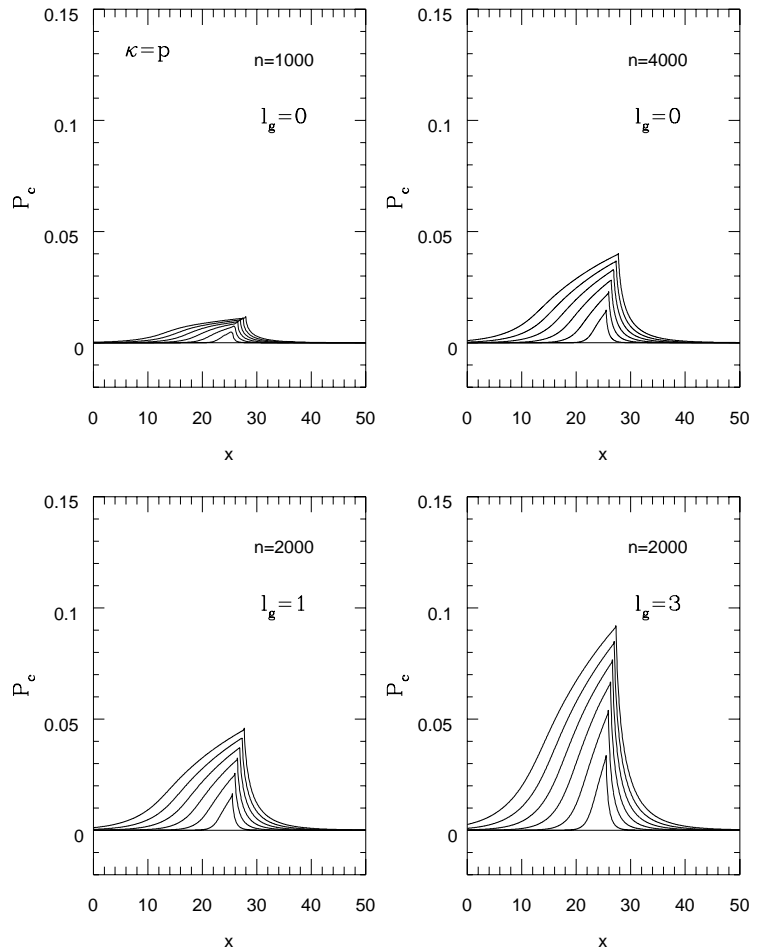
Figure 3: Time evolution of the CR pressure for cases in Fig. 2.

References

Berger, M. J., & LeVeque, R. J. 1998, SIAM J. Numer. Anal., 35, 2298

LeVeque, R. J. 1997, J. Comput. Physics, 131, 327

LeVeque, R. J., & Shyue, K. M. 1995, SIAM J. Scien. Comput. 16, 348

Kang, H., & Jones, T.W. 1991, MNRAS, 249, 439

Kang, H., & Jones, T.W. 1995, ApJ, 447, 944